

EFFECT OF BORON CONTENT ON METALLURGICAL AND MECHANICAL CHARACTERISTICS OF LOW CARBON STEEL

M. EL-SHENNAWY¹, A. I. FARAHAT², M. I. MASOUD³ & A. I. ABDEL-AZIZ⁴

¹Department of Mechanical Engineering, Faculty of Engineering, Helwan University, Helwan, Cairo, Egypt

²Central Metallurgical Research and Development Institute (CMRDI), Helwan, Cairo, Egypt

^{3,4}Industrial Engineering Department, Faculty of Engineering, Fayoum University, Fayoum, Egypt

ABSTRACT

Low carbon bainitic micro alloyed steels containing Nb, Ti and V are widely used for the pipeline, construction and automobile industries because of their excellent combination of strength, toughness and weld ability. Adding boron to this type of steel improves its hardening ability by promoting bainite or martensite formation. This work aims at finding out the effect of different boron content on metallurgical and mechanical properties of low carbon steel. Three alloys were cast with different boron content. Dilatation studies were carried out on these alloys to determine critical transformation temperatures. Tensile, hardness and impact tests were conducted at room temperature. Metallographic investigation using optical and scanning electron microscopes was carried out. Results showed that boron has a strong effect in refining microstructure and ferrite-pearlite features such as layer thickness and distribution. Dilatation behavior exhibited the changes of transformation temperature such as austenite-ferrite, bainite and martensite transformation temperatures.

KEYWORDS: Metallurgical and Mechanical Characteristics of Low Carbon Steel

INTRODUCTION

Low carbon boron-containing steels are widely used in many industrial applications such as gas and oil pipelines, construction and automobile industries because it replaces the high-carbon and low-alloy steels used in a form of sheets and strips with low-cost. These types of steels are also used in a wide variety of applications, such as tools, machine components, and fasteners after cold-forming and heat treatment which enhance hardness and toughness. Boron added to low alloy steel promotes bainite formation by suppressing the austenite transformation, therefore improves its strength and increases the hardenability of the steels [1-7].

The effectiveness of boron in steel decreased with increasing carbon level in the steel [7]. Therefore, boron is most effective in low carbon steels (up to 0.25% C) but is also widely used in medium carbon steels (up to 0.4%C). Adding boron promotes bainite or martensite transformation which increases steel strength. The effect of boron on strengthening can be enhanced by adding certain alloying elements such as molybdenum, niobium and copper by lowering the austenite to ferrite transformation temperature [8-9].

The hardenability of steel can be remarkably increased through addition of boron [7, 10-12]. With an addition of only 0.001- 0.003% soluble boron to low alloy steel, the hardenability of the steel can be improved to a level comparable to that obtained by additions of about 0.5% manganese, chromium or molybdenum. Effect of boron content on mechanical and metallurgical properties in general has been investigated by various researchers [13-15].

The purpose of this work is to find out the effect of different boron contents on the dilatation behavior and metallurgical and mechanical properties of low carbon steel. Dilatation behavior exhibits the changes of austenite-ferrite, bainite and martensite transformation temperatures. Metallurgical properties include grain size, ferrite-pearlite features such as layer thickness and distribution and bainite and martensite morphology. Mechanical properties are investigated through hardness, tensile and impact tests.

EXPERIMENTAL WORK

Casting

Low carbon micro alloyed boron bearing steel was manufactured using open air induction furnace. The steel was in Y-blocks as shown **Figure 1**. Four steel alloys of boron steel containing 0.0003, 0.005, 0.007 and 0.02wt% boron were produced. The chemical composition of the manufactured steel alloys is listed in **Table 1**. Before hot forging, heads of the Y-blocks were removed. Each Y-block was cut into two plates and cleaned from sand.



Figure 1: As Cast Material, Y-Block

Table 1: Chemical Composition in WEIGHT Percent

Alloy	C	Si	Mn	P	S	Cr	Al	B
0.0003B	0.230	0.362	1.13	0.0215	0.0131	0.133	0.117	0.0003
0.005B	0.263	0.339	1.18	0.0242	0.0146	0.137	0.118	0.005
0.007B	0.275	0.306	1.43	0.0295	0.0142	0.052	0.014	0.007
0.02B	0.228	0.356	1.10	0.0215	0.0116	0.132	0.166	0.02

Dilatation Test

To determine the transformation temperatures (A_{c1} , A_{c3} , A_{cme} and A_{c4}), samples from each steel alloy were heated up to 1200°C and tested by dilatometer. On the other hand, empirical formulas [16-18] for calculation of transformation temperatures were used to examine their validation.

$$B_s (^{\circ}\text{C}) = 830 - 270 \text{ C} - 90 \text{ Mn} - 37 \text{ Ni} - 70 \text{ Cr} - 83 \text{ Mo} \quad [16] \quad (1)$$

$$M_s (^{\circ}\text{C}) = 539 - 423 \text{ C} - 30.4 \text{ Mn} - 12.1 \text{ Cr} - 17.7 \text{ Ni} - 7.5 \text{ Mo} \quad [17] \quad (2)$$

$$A_{c1} (^{\circ}\text{C}) = 723 - 10.7 \text{ Mn} - 16.9 \text{ Ni} + 29.1 \text{ Si} + 16.9 \text{ Cr} + 290 \text{ as} + 6.38 \text{ W} \quad [18] \quad (3)$$

$$A_{c3} (^{\circ}\text{C}) = 910 - 203 \text{ SQRT(C)} - 15.2 \text{ Ni} + 44.7 \text{ Si} + 104 \text{ V} + 31.5 \text{ Mo} + 13.1 \text{ W} \quad [18] \quad (4)$$

Mechanical and Metallurgical Tests

Tensile test specimens were extracted from each alloy to examine their mechanical properties according to ASTM E8-01. Charpy impact tests were performed at room temperature according to ASTM E23-01. Hardness test was conducted using a Vickers hardness testing machine. Optical micrographs were taken for specimens from each alloy to examine microstructure characteristics such as grain size, ferrite-pearlite features including layer thickness and distribution and bainite and martensite morphology. New technique for image analysis using AutoCAD program was developed to determine phase volume fraction. Scanning electron microscope was used to clarify grain size and the distribution of the different phases and their morphology.

RESULTS AND DISCUSSIONS

Dilatation

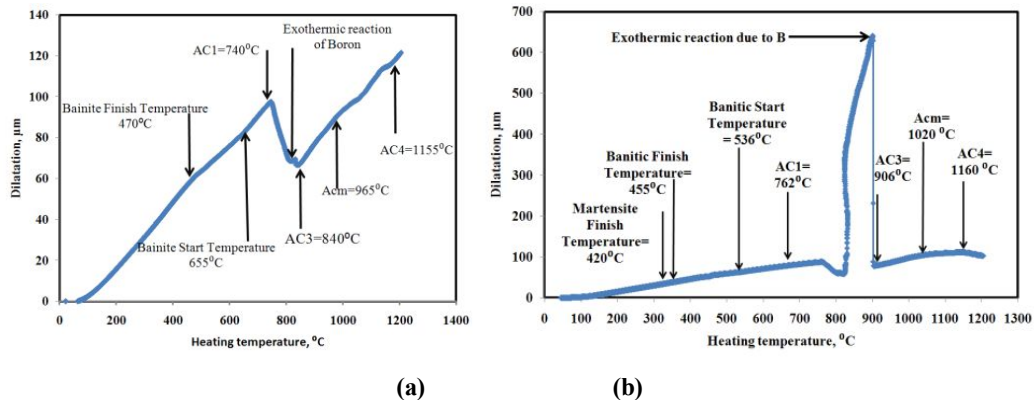
Figure 2 shows a plateau of the general dilatation behavior for different boron steels. It consists of three zones of phase transformations. The first zone is bainite transformation temperatures which include bainite start transformation temperature (B_s) and bainite finish transformation temperature (B_f). The second zone is transformation temperatures from ferrite to austenite (A_{c1} and A_{c3}). The third zone is the dissolution of cementite (A_{cm} and A_{c4}). It is found that the critical transformation temperature A_{c1} exhibits peak before A_{c3} transformation temperature due to the existence of B which produces exothermic reaction peak due to iron boride (Fe-B) dissolution.

From **Figure 2** the actual transformation temperatures were determined. In the same time empirical formulas [16-18] were used to calculate those temperatures. Actual and calculated temperatures are summarized in **Table 2**. It is clear that there is a significant difference between the measured and calculated A_{c1} and A_{c3} . Differences between measured and calculated B_s were negligible. Therefore, the expected transformation temperatures formulas for A_{c1} and A_{c3} are not valid for this type of steel. Selected example for curves of calculated and measured values is shown in **Figure 3**.

Microstructure

0.0003B Steel

Figure 4 shows the as cast microstructure of 0.0003B steel alloy. It consists of mainly polygonal ferrite (white phase) and pearlite (dark phase) as well as a dendrite structure of acicular shapes.



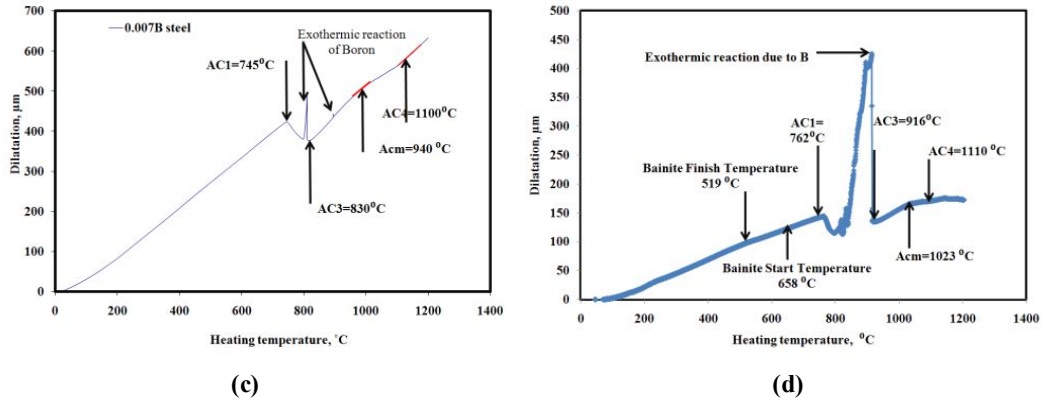


Figure 2: General Dilatation Behavior of Boron Steel for different Boron Content, (a) 0.0003B Steel, (b) 0.005B Steel, (c) 0.007B Steel and (d) 0.02B Steel

Table 2: Expected & Actual Transformation Temperatures

Alloy	Ac ₁		Ac ₃		Bs	
	Predicted	Measured	Predicted	Measured	Predicted	Measured
0.0003B	723.69	740	828.83	840	656.89	655
0.0050B	722.55	762	821.05	903	643.2	650
0.0070B	717.48	745	817.22	830	617.81	-----
0.0200B	723.82	762	828.98	916	660.2	658

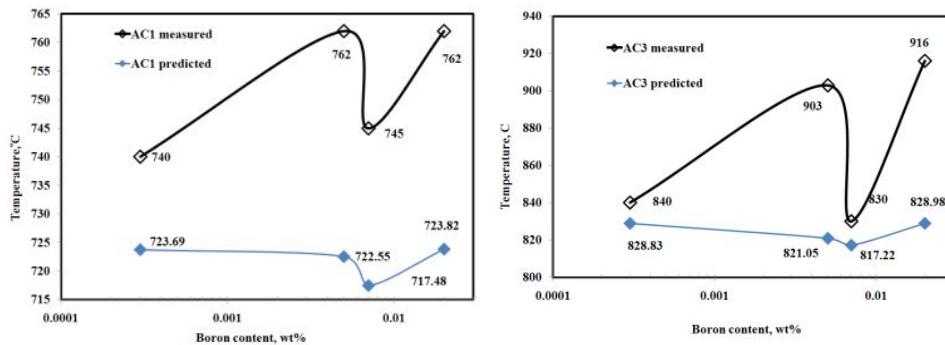
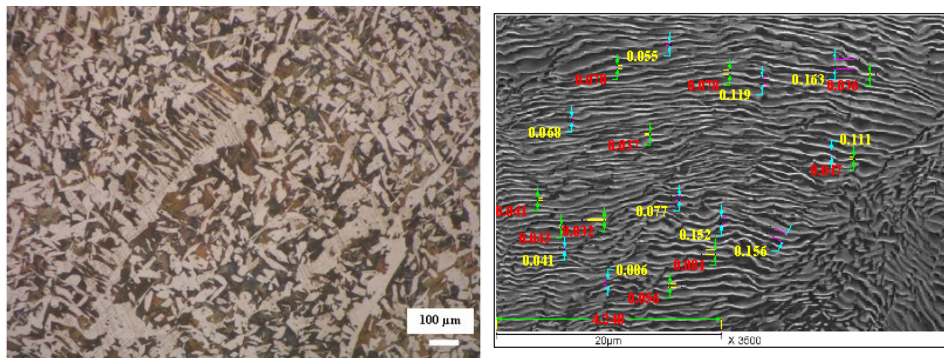


Figure 3: Measured and Calculated Temperatures (Ac₁&Ac₃) for BORON Steel



(a) Optical micrograph

(b) SEM micrograph

Figure 4: Microstructure of the as Cast 0.0003B Steel

Pearlite layers and grain size were determined by image analysis using AutoCAD technique. The pearlite layers thickness are measured by image analysis as shown in **Figure 4 (b)**. It is clear that the average thickness of pearlite carbides is approximately 0.25µm as listed in **Table 3**. The histogram of **Figure 5** shows that approximately 60% of pearlite thickness is in the range of 0.23µm while 40% is in the range of 0.4µm.

Table 3: Statistical Analysis of Pearlite Thickness of 0.0003B Steel

Carbide of Pearlite Thickness, µm	
Mean	0.25
Standard Error	0.03
Median	0.21
Mode	----
Standard Deviation	0.09
Count	10.00
Confidence Level (95.0%)	0.06

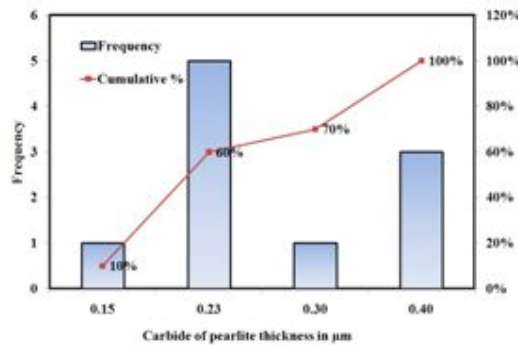


Figure 5: Histogram of Pearlite Thickness Distribution of as-cast 0.0003B Steel

To determine the ferrite and/or pearlite phase ratio (volume fraction %) of 0.0003B steel alloy, image analysis is carried out at x200 as shown in the microstructure of **Figure 6**. It is found that; ferrite to pearlite volume fraction is approximately 58 to 42% as shown in **Figure 7**. Cast boron steel has coarse ferrite and pearlite grains as shown in **Figure 8**. From image analysis and statistical analysis the average ferrite grain size is 34.8µm of 75%. On the other hand, statistical analysis showed that pearlite grain size is approximately 75.1µm, the average inter-lamellar displacement of pearlite is 0.48µm.

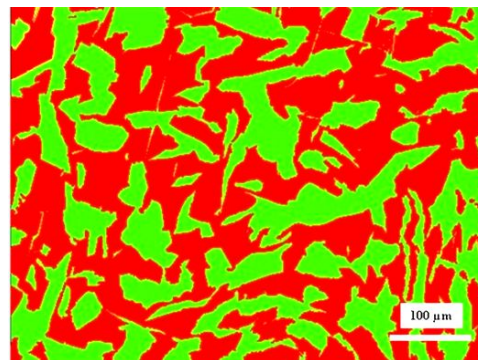


Figure 6: Image Analysis of 0.0003B Steel

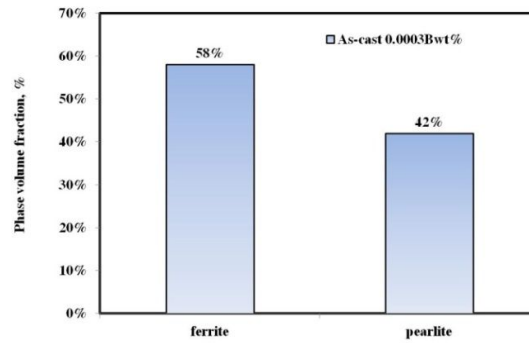


Figure 7: Ferrite-Pearlite Phase Volume Fraction of 0.0003B Steel

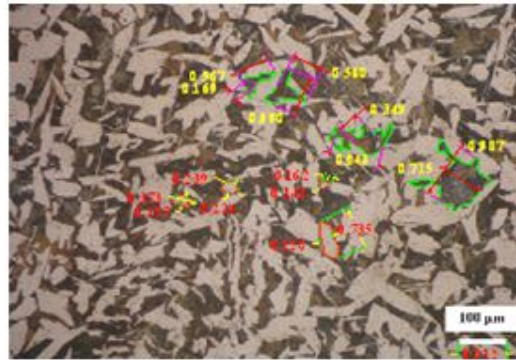


Figure 8: Image Analysis of Ferrite and Pearlite Grain Size of as-Cast 0.0003B Steel

0.005B Steel

Figure 9 shows the as cast optical microstructure of 0.005B steel. It consists of mainly ferrite and pearlite phase. It is clear that microstructure has dendrite structure of acicular shapes due to casting process. To determine the ferrite and/or pearlite phase ratio (volume fraction %) of 0.005B steel alloy as-cast, image analysis was carried out at x200 as shown in Figure 10. From image analysis it is found that ferrite/pearlite volume fraction is approximately 51.45 to 48.55%. Figure 11 shows the Image analysis of ferrite-pearlite grain size and pearlite thickness. It is apparent that, average ferrite grain size of 0.005B steel is approximately 41 μm. It seems clear – after statistical analysis – that about 50% of grain size is less than 45 μm.

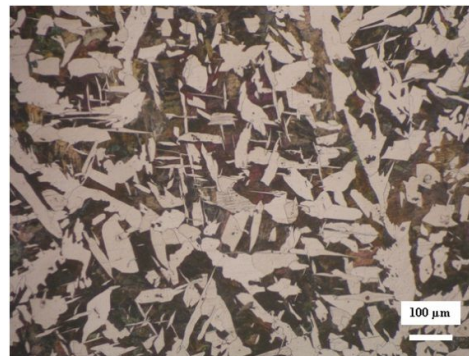


Figure 9: As-Cast Microstructure of 0.005B Steel

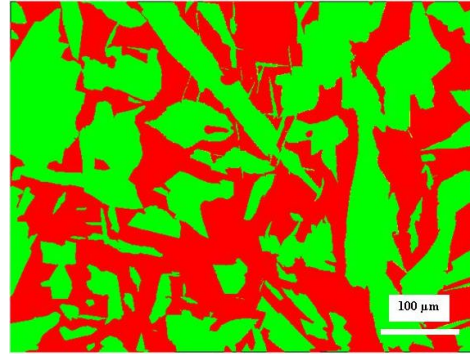


Figure 10: Image Analysis of As-Cast Microstructure of 0.005B Steel

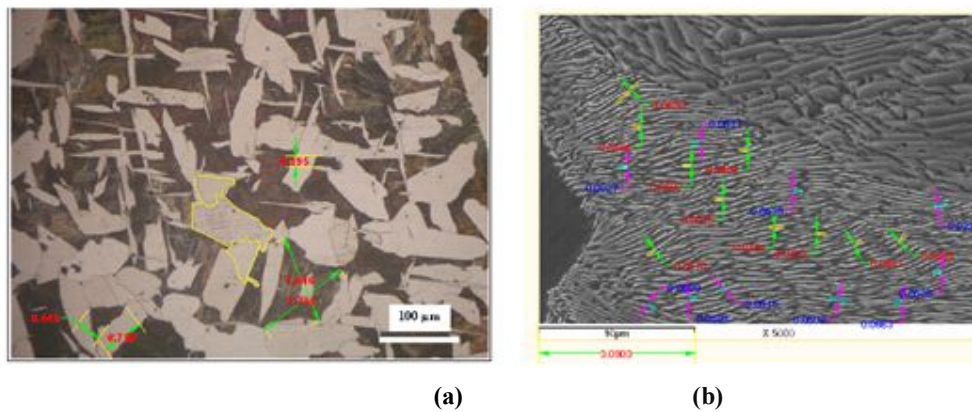


Figure 11: Image Analysis of (a) Ferrite-Pearlite Grain Size and (b) Pearlite Thickness of as Cast 0.005B Steel

The statistical analysis data of the pearlite grain size showed that the average pearlite grain size is $55\mu\text{m}$ while the median value is about $47.1\mu\text{m}$. It showed also that 60% of pearlite has $60\mu\text{m}$ grain size. The average pearlite thickness is $0.2\mu\text{m}$ coinciding with the median. Pearlite thickness distribution showed that about 70% of pearlite exhibits $0.17\mu\text{m}$ thickness. The average inter-lamellar displacement is $0.2\mu\text{m}$ coinciding with the median. Furthermore, there is about 70% of inter-lamellar displacement shows $0.2\mu\text{m}$ thickness.

Microstructure of 0.007B Steel

Figures 12 (a) and (b) shows the optical microstructure of as cast 0.007B steel alloy. It consists of mainly ferrite and pearlite. **Figure 12 (b)** is the optical microstructure of the as-cast at higher magnification. It seems that the grain boundaries are free of any precipitation especially of iron-boride (Fe-B). From image analysis it is found that ferrite/pearlite volume fraction is approximately 29.86 to 70.16%. It is apparent, that boron encourages pearlite phase formation. **Figure 13** shows more details of pearlite layers of 0.007B steel. It is clear that the pearlite layers are thicker than those of 0.005B and also discontinuous. **Figure 14** shows the image analysis of ferrite and pearlite grain size. Statistical analysis showed that the average grain size of ferrite is $58.2\mu\text{m}$ which nearly coincides with median value. It showed also that the ferrite grain size is homogeneously distributed.

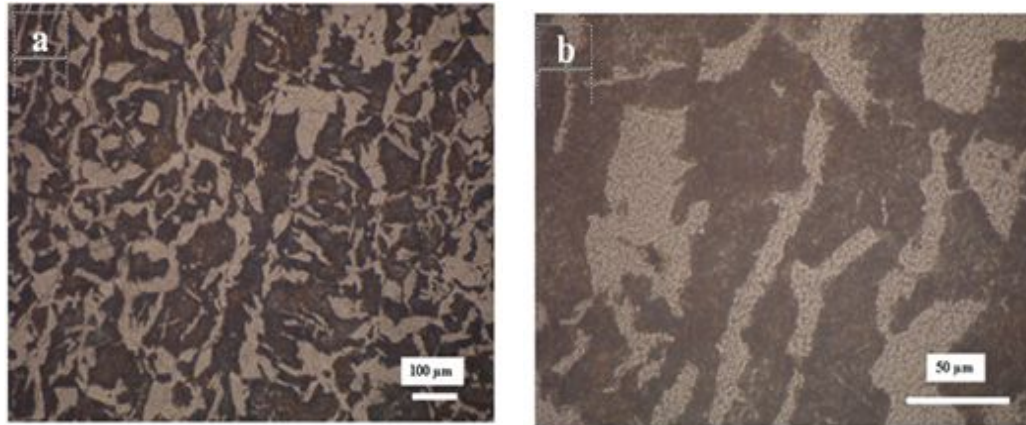


Figure 12: Microstructure of 0.007B Steel

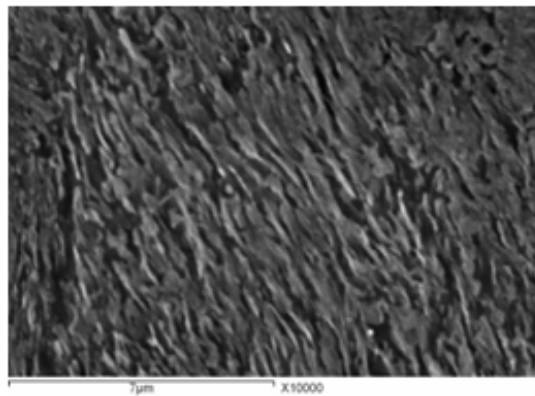


Figure 13: General View of as Cast SEM

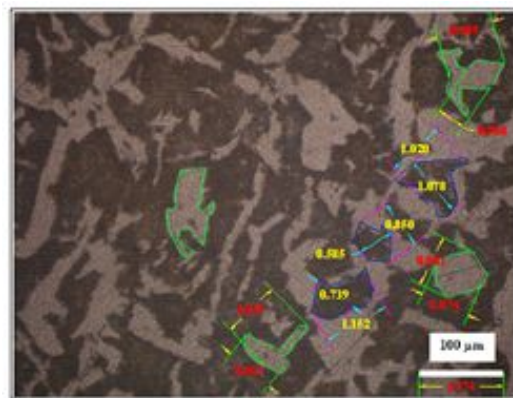


Figure 14: Image Analysis of Ferrite and Microstructure of 0.007B Steel Pearlite grain Size of 0.007B Steel

Statistical analysis showed that the average pearlite grain size is approximately $61.3\mu\text{m}$. It is found that the median nearly equals the average value. It was found that more than 50% of pearlite grains have the average value. **Figure 15** is the image analysis of pearlite thickness. From statistical analysis of pearlite thickness, it is found that the pearlite thickness is $0.25\mu\text{m}$.

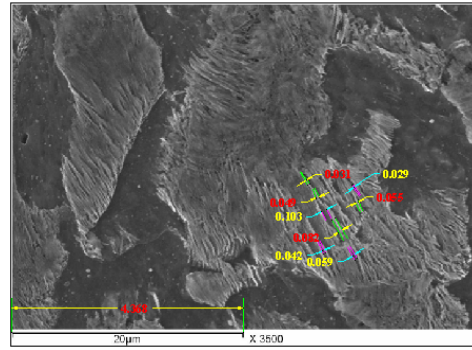


Figure 15: Image Analysis of Pearlite Thickness of 0.007B Steel

Statistical analysis data of the inter-lamellar displacement of pearlite showed that the average inter-lamellar displacement is $0.27\mu\text{m}$ coinciding with the median. Furthermore, there is about 75% of inter-lamellar displacement shows $0.27\mu\text{m}$ thickness.

Microstructure of 0.02B Steel

Figure 16 shows the as cast microstructure of 0.02B steel It consists of mainly ferrite phase and pearlite phase. It is clear that microstructure is dendrite structure of acicular shapes.



Figure 16: As-Cast Microstructure of 0.02B Steel

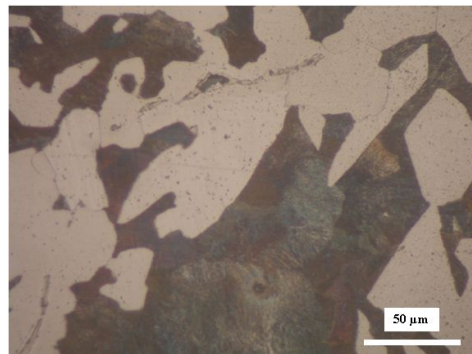


Figure 17: As-Cast Microstructure of as Cast 0.02B Steel

From image analysis it is found that ferrite/pearlite volume fraction is approximately 57.37 to 42.63 %. **Figure 17** shows as-cast optical microstructure of 0.02B steel at x500 magnification, where iron boride (Fe-B) is precipitated at the

grain boundaries of ferrite. The excessive amount of boron forms the compound iron boride. It is well known that iron boride has low melting temperature (hot shortness) that leads to severe cracks during hot deformation. Due to the low stability of grain boundaries (highly disordered structure); the iron boride preferably precipitates at the grain boundaries [19].

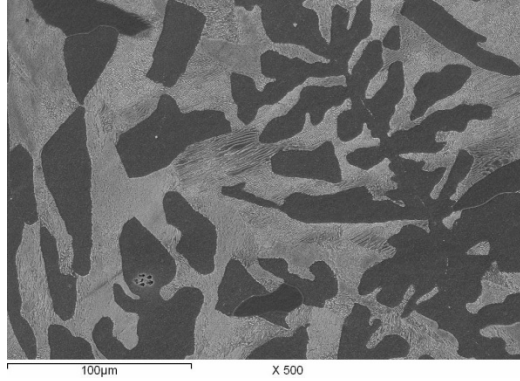


Figure 18: General View of as Cast SEM Micrograph of as Cast 0.02B Steel

To illustrate the distribution of ferrite-pearlite, a general view of as cast SEM micrograph of 0.02B steel is demonstrated in **Figures. 18-19** where the discontinuous net of iron boride appears. Pearlite forms continuous areas. **Figure 20** shows the pearlite morphology. It has thin and intermittent layers of pearlite. From statistical analysis it is found that the grain size of ferrite is $52.63\mu\text{m}$. The average grain size of pearlite is $67.46\mu\text{m}$. **Figure 21** is the image analysis of pearlite phase thickness of as cast SEM micrograph of 0.02B steel. It is found that the average pearlite thickness is $0.21\mu\text{m}$. The average inter-lamellar displacement of pearlite is $0.17\mu\text{m}$.

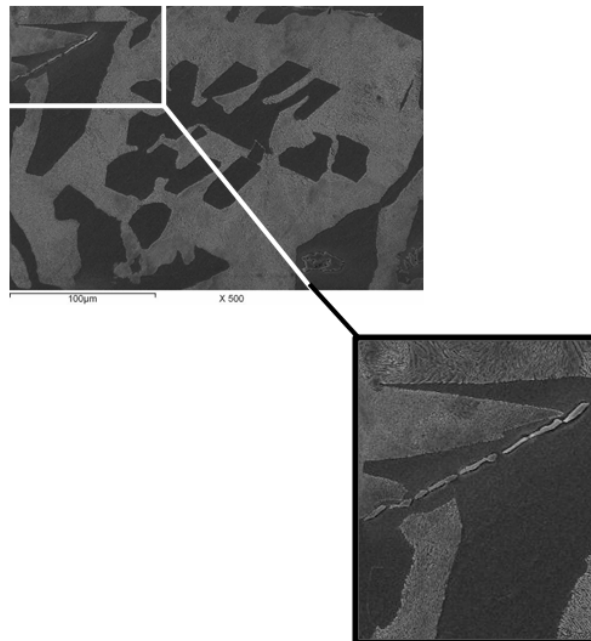


Figure 19: General View of as Cast SEM Micrograph of 0.02B Steel Showing Discontinuous Net of Iron-Boride

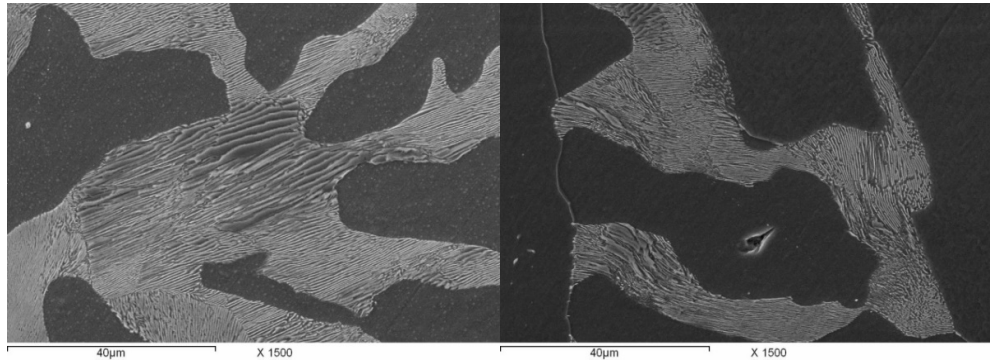


Figure 20: General View of Pearlite of the as Cast SEM Micrograph of as Cast 0.02B Steel

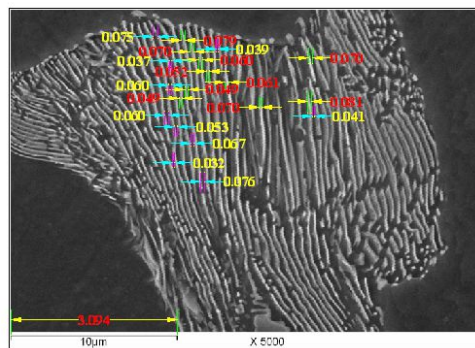


Figure 21: Image Analysis of Pearlite Phase Thickness of as Cast of 0.02B Steel

Hardness Test

Vickers hardness test was carried out at room temperature for steel specimens with various boron contents. **Figure 22** summarizes mean hardness values of as-cast steel for different boron contents. Steel with boron content 0.007 wt% showed the highest hardness value. Both steels with 0.0003 and 0.005 wt% boron exhibited nearly the same hardness values. The decrease in hardness for the alloy containing 0.02 wt% boron may be due to the formation of iron boride.

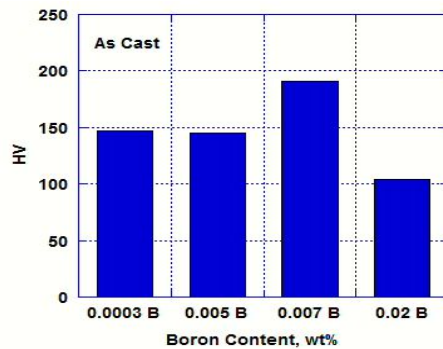


Figure 22: Histogram of Hardness Vickers

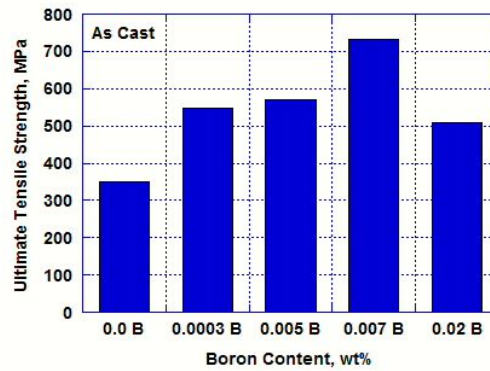


Figure 23: Tensile Strength for Steel with of all Alloys Different Boron Content

Tensile Test

Figure 23 Summarizes mean ultimate tensile strength for steel with different boron content. Almost typical trend was recorded as in case of hardness results. The highest tensile values were recorded for steel with 0.007 wt% boron content. The 0.0003 and 0.005 wt% boron steels had nearly same tensile strength. The minimum tensile strength was recorded with steel with 0.02 wt% boron content. It is important to notice that boron –in general- increased the tensile properties of the steel compared with steel without boron. It is believed that boron existence refined the microstructure which enhanced the tensile and hardness properties when boron contents does not exceed 0.007 wt% for current study. Besides, the increase in volume fraction of pearlite enhanced the tensile properties. For the alloy with 0.02 wt% boron, the effect of grain refinement and volume fraction increase of pearlite was dominant which kept the tensile properties higher than alloy with zero boron content.

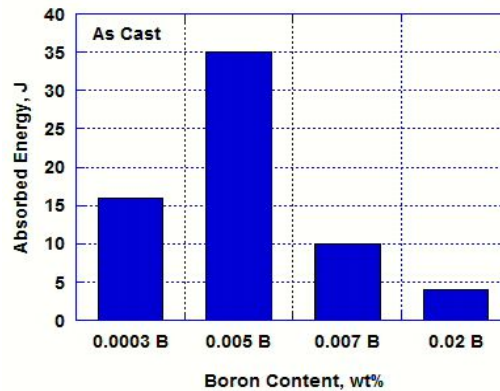


Figure 24: Describes the Impact Behavior versus Boron Content

Impact Test

Figure 24 describes the impact behavior versus boron content. Here it can be noticed that steel with lesser boron, namely 0.005 wt% absorbed the higher energy than other steels either with lower or higher boron content. The worst toughness could be recorded for steel with 0.02 wt% boron. It is expected that iron boride played negative role in minimizing the toughness where cracks were easily initiated due to hot shortness of the iron boride.

CONCLUSIONS

Three alloys were cast with different boron content. Dilatation studies were carried out on these alloys to determine critical transformation temperatures. Tensile, hardness and impact tests were conducted at room temperature. Metallographic investigations using optical and scanning electron microscopes were carried out. From this study the following concluding remarks could be drawn:

- Boron has a strong effect on refining microstructure.
- All cast alloys exhibited microstructure that consists of mainly ferrite and pearlite phase with dendrite structure of acicular shapes due to casting process.
- New technique for calculating phase distribution percentages using Auto Cad has been developed for metallurgical properties' determination
- Boron existence played an important role in changing the ferrite/pearlite ratio in microstructure by increasing the pearlite percentage from 42% to 70% in the expense of ferrite percentage which decreased from 58% to 30%. This behavior was valid for alloys with boron content up to 0.007 wt%.
- Alloy with 0.02 wt% boron showed precipitation of iron boride (Fe-B) in ferrite grain boundary. This is because of low stability of grain boundaries (highly disordered structure).
- Inter-lamellar displacement for alloys with different boron content has been measured and showed larger displacement for alloy with minor boron content, 0.0003 B, namely 0.48 μm . This displacement showed its minimum value with alloy having 0.02 wt% boron, namely 0.17 μm .
- Mechanical properties for alloy with 0.007 wt% boron showed the best values for tensile strength and hardness while alloy with 0.005 wt% boron showed the best toughness property with higher absorption energy value.

ACKNOWLEDGEMENTS

The authors would like to thank Prof. Adel A. Omar, Professor of material science, Benha University and Taif University for his valuable discussion and comments.

REFERENCES

1. P.D. Deeley, K.J.A. Kundig, Review of Metallurgical Applications of Boron Steels, Shield alloy Corporation, Newfield, New Jersey.
2. T.W. Lippert, Boron, the Iron Age, Nov. 19, 1942.
3. R. Walter, British Patent 160, 792, 1921; U.S. Patent!, 519, 388, Aug. 13, 1921.
4. M.A. Grossman, Trans. AIME, 150, pp. 227, 1942.
5. G.F. Comstock, Trans. AIME, 150, pp. 408, 1942.
6. R.A. Grange, Boron in Iron and Steel, Boron, Calcium, Columbium and Zirconium in Iron and Steel Alloys of Iron, Research Monograph Series, John Wiley and Sons, Inc. N.Y., N.Y. p. 3, 1957.

7. B.M. Kapadia, R.M. Brown, W.J. Murphy, *Trans. AIME*, 242, pp. 1689, 1968.
8. K. Yamanaka, Y. Ohmori, Effect of Boron on Transformation of Low Carbon Low Alloy Steels, *Trans, ISIJ*, 17, p. 92, 1977.
9. D. McLean, "Grain boundaries in metals" (Clarendon Press, Oxford, 1957).
10. Ph. Maitrepierre, J. Rafes-Vernis and D. Thivellier: Boron in Steel, ed. by S. K. Banerji and J. E. Morral, AIME, Warrendale, PA, 1979.
11. R. A. Grange and J. B. Mickel: *Trans. Am. Soc. Met.*, 53, p. 15, 1956.
12. M. Deighton, *J. Iron Steel Inst.*, 205, p. 355, 1967.
13. Fábio Dian Murari, André Luiz Vasconcelos da Costa e Silva, Roberto Ribeiro de Avillez, Cold-rolled multiphase boron steels: microstructure and mechanical properties, *Journal of Materials Research and Technology* Volume 4, Issue 2, April–June 2015, Pages 191–196.
14. Stefan Golling, Rickard Östlund, Mats Oldenburg, Characterization of ductile fracture properties of quench-hardenable boron steel: Influence of microstructure and processing conditions, *Materials Science and Engineering: A*, Available online 5 February 2016.
15. M. Naderi, M. Ketabchi, M. Abbasi, W. Bleck^b, Analysis of microstructure and mechanical properties of different high strength carbon steels after hot stamping, *Journal of Materials Processing Technology*, Volume 211, Issue 6, 1 June 2011, Pages 1117–1125.
16. W. Stevens and A.G. Haynes, The Temperature of Formation of Marten site and Bainite in Low-alloy Steel, *JISI*, Vol 183, 1956, p 349–359.
17. K.W. Andrews, Empirical Formulae for the Calculation of Some Transformation Temperatures, *JISI*, Vol 203, 1965, p 721–727.
18. George Krauss, *Steels Processing, Structure, and Performance*, 2005 ASM International.
19. Peter Ernst' Effect of boron on the mechanical properties of modified 12 % chromium steels!, 1988.